CrossMark

Actin dynamics shape microglia effector functions

Ria Uhlemann[1] · Karen Gertz[1,2] · Wolfgang Boehmerle[1] · Tobias Schwarz[1] ·
Christiane Nolte[3] · Dorette Freyer[1] · Helmut Kettenmann[3] · Matthias Endres[1,2,4,5] ·
Golo Kronenberg[1,2,6]

Abstract Impaired actin filament dynamics have been associated with cellular senescence. Microglia, the resident immune cells of the brain, are emerging as a central pathophysiological player in neurodegeneration. Microglia activation, which ranges on a continuum between classical and alternative, may be of critical importance to brain disease. Using genetic and pharmacological manipulations, we studied the effects of alterations in actin dynamics on microglia effector functions. Disruption of actin dynamics did not affect transcription of genes involved in the LPS-triggered classical inflammatory response. By contrast, in consequence of impaired nuclear translocation of phospho-STAT6, genes involved in IL-4 induced alternative activation were strongly downregulated. Functionally, impaired actin dynamics resulted in reduced NO secretion and reduced release of TNFalpha and IL-6 from LPS-stimulated microglia and of IGF-1 from IL-4 stimulated microglia. However, pathological stabilization of the actin cytoskeleton increased LPS-induced release of IL-1beta and IL-18, which belong to an unconventional secretory pathway. Reduced NO release was associated with decreased cytoplasmic iNOS protein expression and decreased intracellular arginine uptake. Furthermore, disruption of actin dynamics resulted in reduced microglia migration, proliferation and phagocytosis. Finally, baseline and ATP-induced $[Ca^{2+}]_{int}$ levels were significantly increased in microglia lacking gelsolin, a key actin-severing protein. Together, the dynamic state of the actin cytoskeleton profoundly and distinctly affects microglia behaviours. Disruption of actin dynamics attenuates M2 polarization by inhibiting transcription of alternative activation genes. In classical activation, the role of actin remodelling is complex, does not relate to gene transcription and shows a major divergence between cytokines following conventional and unconventional secretion.

Keywords Actin cytoskeleton · Gelsolin · Inflammation · Microglia polarization

✉ Matthias Endres
matthias.endres@charite.de

✉ Golo Kronenberg
golo.kronenberg@charite.de

1 Klinik und Hochschulambulanz für Neurologie, Charité Universitätsmedizin Berlin, Charitéplatz 1, 10117 Berlin, Germany

2 Klinik und Poliklinik für Neurologie and Center for Stroke Research Berlin (CSB), Charité Universitätsmedizin Berlin, Charitéplatz 1, 10117 Berlin, Germany

3 Cellular Neuroscience, Max-Delbruck-Center for Molecular Medicine, 13092 Berlin-Buch, Germany

4 Excellence Cluster NeuroCure, 10117 Berlin, Germany

5 German Center for Cardiovascular Research (DZHK), 13347 Berlin, Germany

6 Klinik und Poliklinik für Psychiatrie und Psychotherapie, Charité Universitätsmedizin Berlin, 10117 Berlin, Germany

Introduction

It is only in recent years that the view of actin as a universal and mundane protein has slowly begun to change. A multitude of cellular processes ranging from morphogenesis, cell division and locomotion to intracellular

transport depend on the finely regulated dynamic reorganization of the actin cytoskeleton. Directed remodelling in response to shifting internal and external demands constitutes a fundamental mechanism in eukaryotic cells. A cell with a less manoeuvrable actin cytoskeleton is, therefore, increasingly unable to react effectively to novel challenges (Gourlay and Ayscough 2005). Reduced turnover of filamentous (F)-actin and increased stiffness of the actin cytoskeleton have been associated with cellular senescence and, ultimately, cell death (Wang and Gundersen 1984; Leadsham et al. 2010). Furthermore, a link between reactive oxygen species and actin stabilization has been demonstrated experimentally (Gourlay and Ayscough 2006; Ni et al. 2013). Abnormal bundling and accumulation of filamentous actin have also been implicated in the etiopathogenesis of adult-onset neurodegenerative conditions such as Huntington's disease, stroke, severe epileptic seizures, and most notably, Alzheimer's dementia. Both amyloid-β and phosphorylated tau protein promote actin stabilization (Furukawa et al. 1997; Endres et al. 1999; Fulga et al. 2007; Henriques et al. 2010; Kwan et al. 2012).

Microglia serve as the primary immune cell of the brain. Microglia activation is a hallmark of a number of brain diseases. Microglia engagement within a specific temporospatial disease context may either foster regeneration and confer neuroprotection, or alternatively, promote neurotoxicity and disease progression (Hanisch and Kettenmann 2007; Aguzzi et al. 2013). The functional spectrum of microglia responses is broad. Here, we speculated that disruption of actin dynamics and, in particular, pathological stabilization of the actin network, would profoundly affect a wide range of activated microglia phenotypes. Quite surprisingly, this issue has only scarcely been addressed in the existing literature.

Two main patterns of microglia activation are widely accepted, the so-called M1 (classical, LPS-induced) and M2 phenotypes ('alternatively activated', induced by IL-4). Activated M1 microglia secrete proinflammatory cytokines such as IL-1beta, IL-6 and TNFalpha. Additionally, M1 microglia produce nitric oxide and reactive oxygen species. The M2 phenotype is commonly distinguished by the expression of certain markers such as arginase and chitinase-like protein 3 (YM1), as well as by the increased production of neurotrophic molecules such as insulin-like growth factor 1 (IGF-1) (Olah et al. 2011).

In the current study, we set out to probe the interplay between microglia activation and the dynamic state of the actin cytoskeleton using both pharmacological actin modulators as well as cells derived from gelsolin-deficient mice ($Gsn^{-/-}$) (Witke et al. 1995). Gelsolin is a powerful actin filament severing protein (Sun et al. 1999). $Gsn^{-/-}$ mice, therefore, represent an excellent model system for studying the pathophysiological sequelae of actin filament

stabilization on key aspects of cellular function. We systematically studied the effects of impaired actin dynamics in microglia on (1) mRNA expression of key genes involved in classical and alternative activation; (2) the release of proinflammatory cytokines, IGF-1 and nitric oxide; (3) cell migration, proliferation and phagocytosis; and (4) basal and ATP-induced intracellular calcium levels. Cumulatively, our results yield the unexpected finding that the respective pattern of effects of actin dynamics on microglia function is distinct both as regards M1 and M2 polarization as well as increased and decreased stability of the actin filament network.

Materials and methods

Animals and drug treatments

All procedures conformed to national and institutional guidelines and were approved by an official committee. Mice lacking gelsolin ($Gsn^{-/-}$) have been described in detail previously (Witke et al. 1995; Azuma et al. 1998; Endres et al. 1999). Bromodeoxyuridine (BrdU) was administered intraperitoneally at a dose of 50 mg/kg body weight.

Primary postnatal microglia cultures

Cultures of primary mouse microglia were prepared from newborn mice (P0–3) as described in detail previously (Hellmann-Regen et al. 2013). Briefly, microglial cells were harvested by gentle shake off and seeded at an initial density of 10^6 cells/ml. Cells remained in culture for an additional 24 h before use. The purity of cultures exceeded 98 % as verified by regular flow cytometry analyses with CD11b and CD45 staining (rat anti-mouse CD11b #553312 and rat anti-mouse CD45 #553081: both from BD Biosciences). All experiments were performed in DMEM containing 10 % foetal calf serum, 1 % Pen/Strep, 1 % sodium-pyruvate and 4.5 g/l D-glucose ("complete medium"; all from Biochrom/Merck KGaA). LPS (*Escherichia coli* 055:B5, Sigma-Aldrich) was applied at a concentration of 1 µg/ml (Hellmann-Regen et al. 2013). Unless indicated otherwise, jasplakinolide (Calbiochem/Merck KGaA) was applied at a concentration of 250 nM and cytochalasin D (Sigma-Aldrich) was applied at a concentration of 2 µM. Recombinant murine IL-4 (PeproTech) was used at a concentration of 10 ng/ml.

Cultures of primary adult microglia

The procedure for the cultivation of adult-derived microglia has been described in detail recently (Scheffel et al.

2012). Cell suspensions of adult (<6 months) and aged (>16 months) mouse brains were seeded into 75 cm^2 cell culture flasks containing a monolayer of neonatal astrocytes. This so-called "substrate culture" was derived from neonatal mixed glial cultures of wild-type mice. After the astrocytic monolayer of the neonatal mixed glial culture had reached confluence, loosely attached microglia were gently shaken off and discarded with the medium. Cultures were then washed once with complete medium, incubated with clodronate (200 μg/ml, Santa Cruz Biotechnology) in complete medium (48 h, 37 °C, 5 % CO$_2$) and vigorously shaken (250 rpm, 37 °C, overnight) to deplete any residual neonatal microglia. Cultures were washed once with phosphate-buffered saline (PBS; Gibco/Life Technologies) and once with complete medium and kept in an incubator (37 °C, 5 % CO$_2$) until further use (within 24–48 h). Before the addition of the adult cell suspension, the astrocytic culture received another medium exchange. 24 h after seeding, postnatal mixed glial cultures were washed (3× PBS) and received fresh complete medium. After 7 days, cultures received complete medium with growth factors GM-CSF (5 ng/ml, #14-8331) and M-CSF (10 ng/ml, #14-8983) (both eBioscience). Genotyping PCR of adult microglia cultures derived from $Gsn^{-/-}$ mice showed mutational insertion into the DNA of the gelsolin gene (Supplementary Figure 1) confirming the purity of cultures (i.e., no spillover of neonatal cells into adult cultures).

Ex vivo isolation of adult microglia

All kits were purchased from Miltenyi Biotec. Brains of adult $Gsn^{+/+}$ and $Gsn^{-/-}$ mice were perfused transcardially with 0.9 % saline. Brains were dissociated using the Neural Tissue Dissociation Kit (P) according to the manufacturer's protocol. After dissociation, myelin was removed using Myelin Removal Beads. Finally, for magnetic cell sorting ("MACS") via columns, the cell suspension was incubated with CD11b MicroBeads. For calcium measurements, CD11b$^+$ cells were seeded onto 8-well chambered coverslips (ibidi) 24 h before imaging. For the modified Boyden chamber assay, cells were immediately seeded on FluoroBlok^{TM} Multiwell Inserts (8 μm pore size, Corning Incorporated).

Preparation of oligomeric β-amyloid$_{1–42}$

Amyloid-β (Aβ) protein(1–42)/FITC-coupled Aβ(1–42) (Bachem) was dissolved in ice-cold hexafluoro-2-propanol (HFIP) (Sigma-Aldrich) at a concentration of 1 mM. The solution was then incubated at room temperature for 2 h to allow monomerization and randomization of structure (Chromy et al. 2003). The HFIP was removed by vacuum centrifugation (Fa et al. 2010) using the Eppendorf

concentrator 5301 until a clear peptide film appeared. The film was stored at −80 °C. One day before the cell culture experiment, the peptide film was dissolved in DMSO (Sigma-Aldrich) at a concentration of 10 mM with further dilution to 100 μM in PBS.

MTT assay

Microglia cell viability was assayed by measuring intracellular reduction of the tetrazolium salt 3-(4,5-dimethylthiazol-2-yl)2,5-diphenyl tetrazolium bromide (MTT) to formazan. The MTT labelling agent (Sigma-Aldrich) was added to the cells at a final concentration of 0.5 mg/ml. The converted dye was solubilized in 10 % SDS in 0.01 M HCl and measured at 550 nm with a plate reader (TriStar LB941, Berthold Technologies).

LDH assay

Aliquots of the cell culture medium were collected for analysis of lactate dehydrogenase (LDH) activity as described previously (Koh and Choi 1987).

NO measurements

Nitric oxide (NO) production was quantified as nitrite accumulation using the Griess reagent for nitrite (Sigma-Aldrich) as described previously (Hellmann-Regen et al. 2013). 100 μl of cell culture supernatant was incubated with 100 μl Griess reagent. Absorption was measured at 550 nm with a microplate spectrophotometer (TriStar LB941, Berthold Technologies). The concentration of nitrite in samples was calculated using a standard curve.

Cytokine measurements

The concentrations of IL-6 (R&D Systems), IL-1beta (R&D Systems), TNFalpha (eBioscience), IGF-1 (R&D Systems) and IL-18 (MBL International) were measured in the cell culture supernatant by ELISA. For adult primary $Gsn^{-/-}$ and $Gsn^{+/+}$ microglia, TNFalpha bioactivity was measured using a modified L 929 cytotoxicity assay as described in detail previously (Freyer et al. 1999).

Messenger RNA isolation and quantitative polymerase chain reactions

Total RNA was extracted using the NucleoSpin® Tissue XS kit (Macherey-Nagel). For polymerase chain reaction amplification, we used gene-specific primers (Table 1) and Light Cycler® 480 SYBR Green I Master (Roche Diagnostics). Polymerase chain reaction conditions were as follows: preincubation 95 °C, 10 min; 95 °C, 10 s, primer-

Table 1 Primer sequences used in quantitative real-time polymerase chain reactions

Adam17	Adam17_for	CTC ATC CTG ACC ACT TTG GTG C	Adam17_rev	GTG TGT CGC AGA CTG TAG ATC C
Arg1	Arg1_for	ATG TGC CCT CTG TCT TTT AGG G	Arg1_rev	GGT CTC TCA CGT CAT ACT CTG T
Arpc5	Arpc5_for	TCT GGA CAA GAA CGG TGT GG	Arpc5_rev	GTG AAC GGT GTC CAG TTC CA
Asl	Asl_for	TAC ACA CAG GAC GAA GTC GC	Asl_rev	TGA ATC TCG TGT CAG CGC AA
Ass1	Ass1_for	GCC AAG TGT ACA TCC TCG GT	Ass1_rev	GAC CTT GCT CTG AAG GCG AT
Cat1	Cat-1_for	CTC TCT CTG CGC ACT TTC CA	Cat-1_rev	CTG AGG TCA CAG TGG CGA TT
Cat2	Cat2_for	ACA ACG GGT GAA GAG GTT CG	Cat2_rev	CCA TCC TCC GCC ATA GCA TA
Cat3	Cat-3_for	CCT ACG TCA TTG GTA CAG CCA G	Cat-3_rev	CAG CAA TCC AGT GAG CAG CAA C
Cfl1	Cfl1_for	TCT GTC TCC CTT TCG TTT CC	Cfl1_rev	ACC GCC TTC TTG CGT TTC TT
Fizz1	Fizz1_for	GTC CCA GTG AAT ACT GAT GAG AC	Fizz1_rev	GTT GCA AGT ATC TCC ACT CTG G
Golga4	p230_for	GAC CAG CTT GAT GAC GTG ACA C	p230_rev	CCT CGC TCT CCA TAT CAG AAG G
Gsn	Gsn_ for	CTC CGT ACC GCT CTT CAC TG	Gsn_rev	CTC ATC CTG GCT GCA TTC ATT G
Igf1	Igf1_for	GTC TTC ACA CCT CTT CTA CCT G	Igf1_rev	GCT GCT TTT GTA GGC TTC AGT G
Il12	IL12b_for	CCG GAC GGT TCA CGT GCT CA	IL12b_rev	CAC TGC CCG AGA GTC AGG GGA
Il18	IL18_for	GAC TCT TGC GTC AAC TTC AAG G	IL18_rev	CTC GAA CAC AGG CTG TCT TTT G
Il1b	IL1b_for	CAA CCA ACA AGT GAT ATT CTC CAT G	IL1b_rev	GAT CCA CAC TCT CCA GCT GCA
Il6	IL6_for	GAG GAT ACC ACT CCC AAC AGA CC	IL6_rev	AAG TGC ATC ATC GTT GTT CAT ACA
Mrc1	Mrc1_for	GTC AGA ACA GAC TGC GTG GA	Mrc1_rev	AGG GAT CGC CTG TTT TCC AG
Nfkb1	Nfkb1_for	GTC AAC AGA TGG CCC ATA CCT TC	Nfkb1_rev	GTC CTG CTG TTA CGG TGC ATA C
iNos	iNOS_for	GCT CGC TTT GCC ACG GAC GA	iNOS_rev	AAG GCA GCG GGC ACA TGC AA
Otc	Otc_for	GTA CTC GAA CAA GAC TGT CCA C	Otc_rev	GCT AAC ACT GCA TCT GTC ATG C
Pfn1	Pfn1_for	TGG AAC GCC TAC ATC GAC AG	Pfn1_rev	TTG CCT ACC AGG ACA CCA AC
Srf	SRF_for	GCT ACA CGA CCT TCA GCA AGA G	SRF_rev	CAG GTA GTT GGT GAT GGG AAA G
Tnfa	TNFa-1_for	CCA CCA CGC TCT TCT GTC TA	TNFa-1_rev	AGG GTC TGG GCC ATA GAA CT
Tpp2	Tpp2_for	CTT CTA TCC AAA GGC TCT CAA GG	Tpp2_rev	CTC TCC AGG TCT CAC CAT CAT G
Vil1	Vil1_for	AGG CTC TCT CAA CAT CAC CAC	Vil1_rev	GTC CTG GCC AAT CCA GTA GT
Ym1	Ym1_for	CTC TAC TCC TCA GAA CCG TCA G	Ym1_rev	GCA GCC TTG AAA TGT CTT CTC C

specific annealing temperature, 10 s, 72 °C, 15 s (45 cycles). Crossing points of amplified products were determined using the Second Derivative Maximum Method (Light Cycler 480 Version 1.5.0, Roche). Quantification of messenger RNA expression was relative to tripeptidyl peptidase (*Tpp*) 2 (Nishida et al. 2006). The specificity of polymerase chain reaction products was checked using melting curve analysis. PCR products were run on a 1.5 % agarose gel to demonstrate the presence of a single amplicon of the correct size. Furthermore, negative controls (i.e., reaction mix lacking either template DNA or reverse transcriptase) yielded no bands on the gel.

Western blotting

Cells were fractionated into cytosolic, membrane and cytoskeletal (pellet) fractions using the Subcellular Protein Fractionation Kit for Cultured Cells (Pierce Biotechnology) according to the manufacturer's protocol. Protein concentration was determined by BCA Protein Assay (Pierce Biotechnology). Equal amounts of protein were loaded on 10 % SDS–polyacrylamide gels (Pierce Biotechnology) and blotted onto polyvinylidene fluoride membranes for 90 min at 100 V using the Trans-Blot® SD semi-dry transfer cell system (Bio-Rad Laboratories). In the experiments investigating IL-4/STAT6 signalling (Fig. 4), purity and equal loading of nuclear and cytosolic fractions were confirmed by histone deacetylase 1 (HDAC1) and GAPDH, respectively. Blots were probed with primary antibodies overnight at 4 °C. HRP-conjugated secondary antibodies were applied for 2 h at room temperature on the following day. As a control, to rule out unspecific binding or false positive signals due to the secondary antibody, the primary antibody was omitted from one strip of the membrane. Proteins were visualized by an enhanced chemiluminescent detection method (Super Signal West Dura Chemiluminescent Substrate, Pierce Biotechnology). Antibodies were used in the following dilutions: rabbit anti-β-actin (Cell Signalling #4967) 1:5000, mouse anti-GAPDH (Millipore #MAB374) 1:5000, rabbit anti-iNOS (M19, Santa Cruz Biotechnology) 1:200, rabbit anti-Gelsolin (Abcam #ab74420) 1:1000, rabbit anti-SRF (Abcam #ab53147) 1:200, rabbit anti-Cofilin (Cell Signalling #3312) 1:800, rabbit anti-Phospho-Cofilin (Cell

Signalling #3311) 1:500, rabbit anti-STAT6 (Cell Signalling #9362) 1:500, rabbit anti-Phospho-STAT6 (Cell Signalling #9361) 1:500, rabbit anti-HDAC1 (Cell Signalling #2062) 1:500, rabbit anti-Phospho-eIF2alpha (Cell Signalling #9721) 1:500, rabbit anti-eIF2alpha (Cell Signalling #9722) 1:500 horseradish peroxidase-conjugated goat anti-mouse IgG (Pierce Biotechnology) 1:2000 and horseradish peroxidase-conjugated goat anti-rabbit IgG (Pierce Biotechnology) 1:2000.

^{14}C-labelled L-arginine uptake studies

Briefly, arginine uptake into microglia was measured after 45 min preincubation with 250 nM jasplakinolide or 2 μM cytochalasin D followed by 6-h cotreatment with LPS. Cells were washed twice with 500 μl prewarmed (37° C) wash buffer [137 mM NaCl, 5.4 mM KCl, 1.2 mM $MgSO_4 \cdot 7H_2O$, 2.8 mM $CaCl_2 \cdot 2H_2O$, 10 mM HEPES and 1 mM KH_2PO_4 (pH 7.4)]. Cells were then resuspended in 250 μl of 50 μM L-[^{14}C(U)]arginine] (274.3 mCi/mmol, 0.1 mCi/ml; Perkin-Elmer) prewarmed wash buffer supplemented with 5 mM L-leucine. The reaction was stopped after 10 min. Samples were washed three times with ice-cold stop solution [10 mM HEPES, 10 mM Tris, 137 mM NaCl, 10 mM nonradioactive L-arginine (pH 7.4)]. Cells were then lysed with 1 % sodium dodecyl sulphate, and radioactivity was counted in a liquid scintillation counter (Wallac 1414, Perkin Elmer).

Microglial phagocytosis

Phagocytosis of bacterial particles was assessed using the pHrodo^{TM} Red *S. aureus* Bioparticles® Conjugate for Phagocytosis (Life Technologies) according to the manufacturer's manual. Postnatal microglia were pretreated with cytoskeletal drugs for 45 min before experimentation. For the Aβ phagocytosis studies, 5 μM FITC-coupled oligomeric Aβ (Bachem) was added to the microglia cultures. After incubation for 2 h at 37 °C, cultures were stained with NucBlue® Live ReadyProbes® Reagent containing Hoechst 33342 (Life Technologies) for 20 min at room temperature. After washing with live cell imaging solution (Molecular Probes/Life Technologies), extracellular fluorescence was quenched by addition of 0.4 % trypan blue solution (Gibco/Life Technologies). FITC and Hoechst fluorescence were measured at wavelengths of 485(ex)/535(em) and 340(ex)/460(em), respectively.

Modified Boyden chamber assay

Cells were seeded onto FluoroBlok^{TM} Inserts (8 μm pore size, Corning Incorporated) at a density of 15×10^3 cells/transwell insert. 100 μM ADP (Sigma-Aldrich) was added to the well below the insert. After 6 h of incubation at 37 °C and 5 % CO_2, the membranes of the inserts were stained with 10 μm CFSE dye (Sigma-Aldrich), and then fixed with 4 % paraformaldehyde (PFA) and counterstained with 2 μm 4′,6′-diamidino-2-phenylindole (DAPI) (Sigma-Aldrich). Migrated cells below the FluoroBlok membranes were visualized using an inverted fluorescence microscope (Leica DMI3000). The rate of microglia migration was calculated by counting cells in four different microscope fields of each membrane (at 200× magnification). In order to account for basal microglia migration, data are presented as the ratio of microglia migration to ADP/microglia migration without ADP.

Calcium imaging

Ex vivo-isolated microglia were seeded onto eight-well μ-Slides (Ibidi) at a density of 3×10^4 cells/well. 24 h after seeding, experiments were performed in HEPES buffer (130 mM NaCl, 4.7 mM KCl, 1 mM $MgSO_4$, 1.2 mM KH_2PO_4, 1.3 mM $CaCl_2$, 20 mM Hepes, 5 mM glucose, pH 7.4). Cells were loaded with Fura-2/AM (5 μM; stock solution dissolved in 20 % pluronic F-127) (Molecular Probes/Life Technologies) by incubation in HEPES buffer at 37 °C for 30 min. After loading, Fura-2 was allowed to de-esterify for at least 10 min at room temperature in standard solution. Cells were monitored with an inverted Olympus IX71 stage equipped with an UPLSAPO X2 40×/ 0.95 objective (Olympus). Fluorescence data were acquired on a PC running xcellence software (Olympus) via a cooled CCD camera (ORCA, Hamamatsu). For stimulation experiments, 100 μM freshly prepared ATP was applied. Intracellular free Ca^{2+} concentration [$(Ca^{2+})_{int}$] was derived from background-subtracted F340/F380 fluorescent ratios (R) after in situ calibration according to the following equation: $[Ca^{2+}]_{int}$ (nM) $= K_d \cdot Q \cdot (R - R_{min})/(R_{max} - R)$, where K_d is the dissociation constant of Fura-2 for Ca^{2+} at room temperature (225 nM); Q is the fluorescence ratio of the emission intensity excited by 380 nm in the absence of Ca^{2+} to that during the presence of saturating Ca^{2+}; and R_{min} and R_{max} are the minimal or maximal fluorescence ratios, respectively. R_{min} was measured by perfusion with Ca^{2+}-free HEPES buffer (as described above) containing 10 μM ionomycin (Sigma-Aldrich). R_{max} was obtained by perfusion with standard solution containing 10 mM $CaCl_2$/10 μM ionomycin. The increase in intracellular Ca^{2+} was calculated by subtracting baseline Ca^{2+} and plotted over time. Ionomycin (viability control after ATP measurements) was applied at 10 μM (not shown).

Facial nerve axotomy

For facial nerve axotomy, we used 6- to 8-week-old $Gsn^{+/+}$ and $Gsn^{-/-}$ mice. The experimental procedures including subsequent histological analyses have been described in detail previously (Pannasch et al. 2006).

Induction of cerebral ischaemia

Mice were anaesthetized with 1.5 % isofluorane and maintained in 1 % isofluorane in 69 % N_2O and 30 % O_2 using a vaporizer. Ischaemia was induced by 30 min filamentous middle cerebral artery occlusion (MCAo)/ reperfusion as described in detail previously (Kronenberg et al. 2005).

Histological procedures, quantification and imaging

The immunohistological procedures including incubation times and temperatures have been described in detail elsewhere (Kronenberg et al. 2003). Briefly, after transcardial perfusion with 0.9 % saline followed by 4 % paraformaldehyde in 0.1 mol/l phosphate buffer, brains were stored in the fixative for 48 h and then transferred into 30 % sucrose in 0.1 mol/l phosphate buffer for 24 h. Coronal sections of 40 μm thickness were cut from a dry ice-cooled block on a sliding microtome (Leica Biosystems). Sections were stored at −20 °C in cryoprotectant solution containing 25 % ethylene glycol, 25 % glycerin and 0.05 mol/l phosphate buffer. All antibodies were diluted in Tris-buffered saline containing 0.1 % Triton X-100 (Sigma-Aldrich) and 3 % donkey serum (Gibco/Life Technologies). Primary antibodies were rat anti-BrdU (Harlan Sera Lab) 1:500, rabbit anti-Iba1 (Wako Chemicals) 1:500 and rabbit anti-Ki67 (Novocastra/Leica Biosystems) 1:100. FITC- or RhodX-conjugated secondary antibodies (from the AffiniPure Donkey Anti-Mouse IgG (H+L) series; Jackson ImmunoResearch Laboratories) were all used at a concentration of 1:250. Confocal microscopy was performed using a spectral confocal microscope (LSM 700; Carl Zeiss Microscopy). Appropriate gain and black level settings were corroborated using negative control slices. These slices were only stained with secondary antibodies, but not with primary antibodies (Glass et al. 2005).

Statistics

Experiments were carried out in a blinded fashion. Data are presented as mean ± SD. Unless otherwise indicated, groups were compared by ANOVA with level of significance set at 0.05 and two-tailed p values using GraphPad Prism 6 (GraphdPad Software).

Fig. 1 Actin dynamics and the mRNA and protein expression of ▶ actin-regulating molecules in activated microglia. Viability of primary mouse microglia as assessed by MTT dye assay (**a**) and LDH release (**b**) was not affected by treatment with either cytochalasin D or jasplakinolide for 24 h at the concentrations used in subsequent experiments (*highlighted* by *grey bars*). However, at higher concentrations, toxic effects were observed for both cytoskeletal drugs. LPS was applied at 1 μg/ml for 24 h as indicated. *$p < 0.05$ relative to respective controls (i.e., cells not treated with cytochalasin D or jasplakinolide). $N = 3$–5 independent measurements per data point. Western blot of protein extracts of non-LPS and LPS-exposed BV-2 microglial cells after 6 h (**c**) and 24 h (**d**) probed with antibodies against gelsolin, phospho-cofilin and cofilin. Note downregulation of phospho-cofilin in the presence of both cytoskeletal drugs (cytochalasin D, 2 μM; jasplakinolide, 250 nM) as well as strong upregulation of gelsolin in the presence of jasplakinolide (**d**). By contrast, activation of cells with LPS did not result in upregulation of actin-binding proteins. Comparable loading of protein is confirmed by GAPDH staining. **e** Analysis of mRNA expression of key genes involved in actin cytoskeleton organization. Primary microglia were exposed to cytoskeletal drugs (cytochalasin D, 2 μM; jasplakinolide, 250 nM) for 6 h. Note that activation of microglia with LPS did not increase mRNA transcription of any of the genes investigated. By contrast, disruption of actin filament dynamics resulted in an overall pattern characterized by increased gene transcription independent of activation status. $N = 4$–5 independent measurements per data point. Two-way ANOVA followed by Tukey's multiple comparisons test. *$p < 0.05$ within LPS/non-LPS treatment condition; #$p < 0.05$ between LPS and non-LPS treatment condition

Results

Disruption of actin dynamics, but not LPS activation, alters the expression of actin-regulating proteins

In an initial dose-finding experiment, the viability of primary postnatal mouse microglia in response to cytoskeletal drugs cytochalasin D and jasplakinolide was assessed after 24 h incubation. Both compounds are cell permeable and serve as pharmacological tools to study the effects of actin depolymerization or increased actin filament stabilization, respectively (Casella et al. 1981; Goddette and Frieden 1986; Bubb et al. 2000; Holzinger 2001). Experiments were performed in the presence or absence of LPS. In the lower concentration ranges used in subsequent experiments, no significant effects on MTT production and LDH release were apparent. However, at higher concentrations, cytotoxicity was observed with both agents (Fig. 1a, b).

Activation of BV-2 microglia with LPS failed to elicit an increase in the protein expression of actin-binding proteins gelsolin and cofilin after 6- and 24-h incubation (Fig. 1c, d). Similar to gelsolin, cofilin is an actin-binding molecule which induces the disassembly of actin filaments (Loisel et al. 1999). Total cofilin levels in brain did not remarkably differ between treatments. However, phosphorylated cofilin, which lacks actin depolymerizing
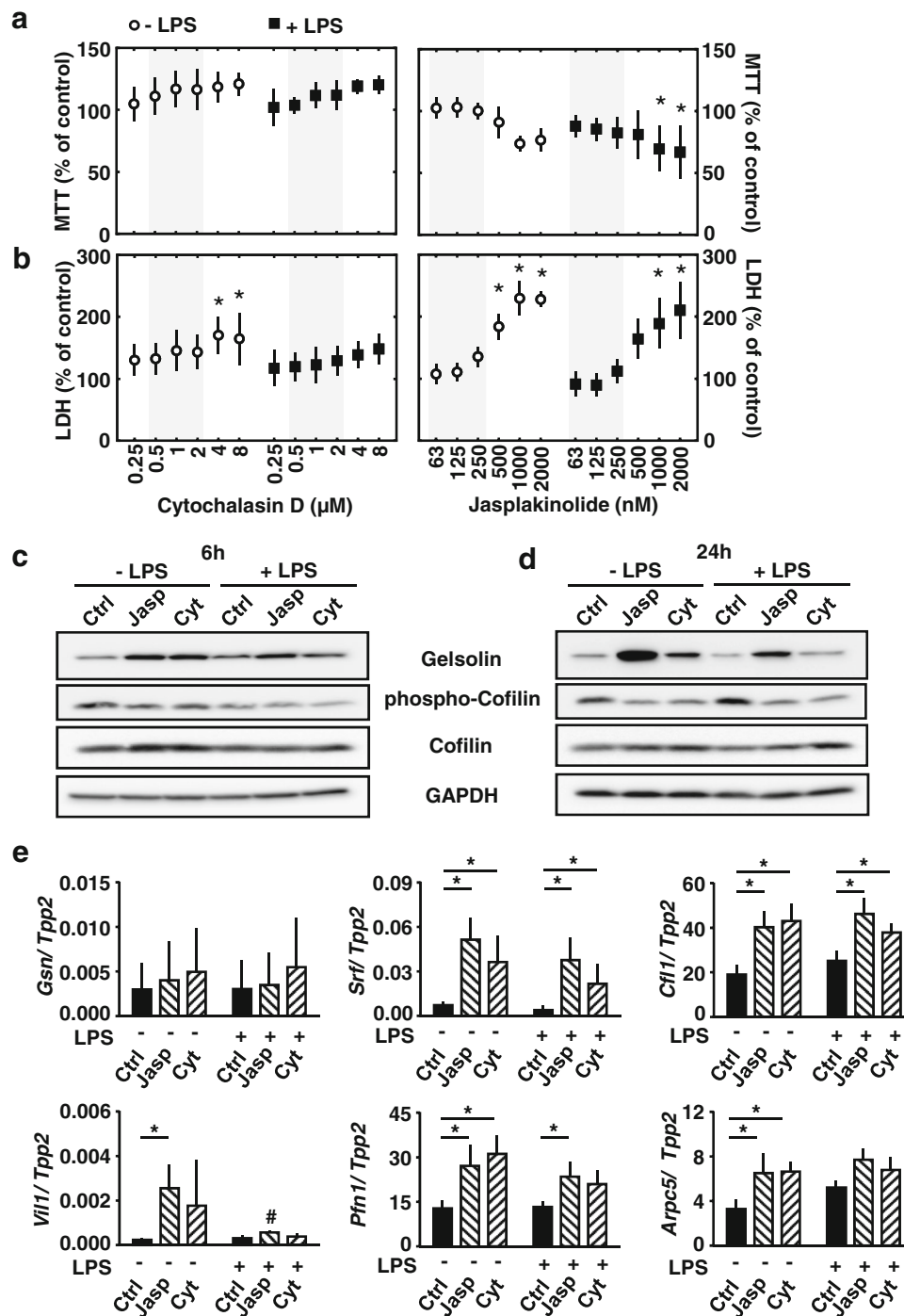
activity (Morgan et al. 1993), was reduced in the presence of both cytoskeletal drugs. In parallel, both actin-binding compounds induced gelsolin expression, an effect which was particularly prominent after 24-h incubation with jasplakinolide (Fig. 1c, d).

Messenger RNA expression of gelsolin (*Gsn*), serum response factor (*Srf*), cofilin 1 (*Cfl1*), villin 1 (*Vil1*), profilin 1 (*Pfn1*) and actin-related protein 2/3 complex subunit 5

(*Arpc5*), key genes associated with actin cytoskeleton organization, was assessed in primary postnatal microglia after 6-h stimulation. Interestingly, activation with LPS did not increase mRNA transcription of any of the genes investigated. However, pharmacological disruption of actin filament dynamics resulted in increased gene transcription independent of stimulation with LPS (Fig. 1e). A similar pattern of gene regulation emerged when alternative

microglia activation was studied. While exposure to IL-4 (10 ng/ml, 24 h) failed to elicit a response, both cytoskeletal drugs again induced upregulation of actin-associated genes (not shown).

Disruption of actin filament dynamics impairs LPS-induced microglial NO release

Production of nitric oxide (NO) is a hallmark of classical microglia activation. LPS-induced NO release from activated primary postnatal mouse microglia was significantly and dose-dependently inhibited by both jasplakinolide and cytochalasin D (Fig. 2a). NO release from gelsolin-deficient microglia harvested from adult and aged mouse brain is illustrated in Fig. 2b.

Activated microglia produce NO from the amino acid L-arginine via inducible nitric oxide synthase (iNOS). Transcription of *iNos* mRNA was significantly upregulated after 6-h LPS stimulation, but was not influenced by co-treatment with either cytoskeletal drug (Fig. 2c). Cationic amino acid transporters (CAT-1, -2 and -3) serve as the principal arginine transporters in most tissues and cells (Macleod and Kakuda 1996). Arginine is not only a substrate for iNOS, but also for arginase (ARG1), an enzyme belonging to the urea cycle that is upregulated by M2 microglia (Colton 2009). Argininosuccinate lyase (ASL), argininosuccinate synthase 1 (ASS-1) and ornithine transcarbamoylase (OTC) are further urea-cycle enzymes. Of the three cationic amino acid transporters, only *Cat2* expression was significantly induced in LPS-activated microglia. By contrast, *Asl* and *Arg1* were downregulated by LPS. Co-treatment with jasplakinolide or cytochalasin D did not affect any of these LPS-regulated genes (Fig. 2c). Expression of *Cat1*, *Cat3*, *Ass1* and *Otc* was not increased in activated microglia (not shown). Taken together, NO production by LPS-stimulated microglia is associated with increased mRNA expression of substrate transporter *Cat2* and of *Nos2*. At the same time, alternative degradation of arginine via arginase is repressed. Remarkably, however, disruption of actin dynamics does not modify the effects of LPS on the transcription of key genes related to increased nitric oxide production by activated microglia.

Next, we studied iNOS protein levels using Western blotting. LPS challenge led to an upregulation of iNOS in BV-2 and in primary postnatal microglia cells (Fig. 2d). Inducible NOS protein was detected in both the membrane and the cytosolic fractions of cell lysates. Interestingly, and in contrast to their effects on *iNos* mRNA concentrations, both cytoskeletal drugs decreased iNOS protein expression in activated microglia. Neither G- nor F-actin levels were affected by LPS activation. However, expectedly, F-actin levels were robustly increased by incubation in the presence of jasplakinolide (Fig. 2d). Protein expression of

Fig. 2 Actin filament dynamics and microglial NO release. Primary postnatal mouse microglia (**a**) and microglia cultured from adult (<6 months, "young") and aged (>16 months, "old") $Gsn^{+/+}$ and $Gsn^{-/-}$ brains (**b**) were stimulated with LPS (1 µg/ml; +) or vehicle (−) for 24 h. $N = 3$–5 independent measurements per data point. **c** Regulation of genes involved in arginine transport and turnover in primary postnatal microglia at 6 h after LPS stimulation. While LPS significantly induced *iNos* and *Cat2* mRNA expression, we did not observe any effect of either cytoskeletal drug. $N = 4$–5 independent measurements per data point. Western blots of protein extracts of non-LPS and LPS-exposed BV-2 (*left* in **d**, **e**) and primary postnatal (*right* in **d**) microglia cells after 6 h. Note strong LPS-induced upregulation of iNOS in the cytosolic fraction which is attenuated by both jasplakinolide (250 nM) and cytochalasin D (2 µM). In the corresponding cytoskeletal ("pellet") fractions, the actin polymerizing and stabilizing effects of jasplakinolide are reflected by increased filamentous (F)-actin levels. **e** Overall eIF2alpha protein concentrations did not differ significantly across experimental groups. However, independent of LPS stimulation, co-treatment with actin stabilizing agent jasplakinolide increased phosphorylation of eIF2alpha. **f** Measurement of the uptake of ^{14}C-L-arginine (disintegrations per minute; dpm) into primary postnatal microglia after 6 h preincubation with LPS. $N = 5$ independent measurements per data point. **g** Treatment with cytoskeletal drugs impairs phagocytosis of FITC-coupled oligomeric Aβ (1–42). Nuclear counterstaining with Hoechst 33342 was performed to confirm equal seeding densities. $N = 7$ independent measurements per data point. **h** In line with reduced phagocytosis of Aβ (1–42), cells treated with cytoskeletal drugs showed significantly reduced *iNos* mRNA expression after 6 h incubation with 10 µM oAβ. $N = 3$ independent measurements per data point. One-way ANOVA followed by Dunnett's post hoc test (**a**, **g**) or two-way ANOVA followed by Tukey's post hoc test (**b**, **c**, **f**, **h**). *$p < 0.05$ within LPS/non-LPS treatment condition; #$p < 0.05$ between LPS and non-LPS treatment condition

iNOS may be regulated at the translational level by phosphorylation of the eukaryotic translation initiation factor 2 (eIF2alpha). An increase in eIF2alpha phosphorylation has been shown to decrease iNOS protein expression (Lee et al. 2003). Here, we found a profound increase in the amount of phosphorylated eIF2alpha in the presence of the actin-stabilizing agent jasplakinolide. However, overall levels of eIF2alpha did not differ between experimental groups (Fig. 2e).

In turn, substrate availability of arginine has been shown to affect eIF2alpha phosphorylation (Lee et al. 2003). We, therefore, also measured L-(14C)-arginine uptake into primary postnatal microglia. Arginine uptake was strongly increased after LPS stimulation. Co-treatment with jasplakinolide resulted in significantly decreased L-(14C)-arginine uptake by activated microglia (Fig. 2f).

Finally, oligomeric Aβ has also been shown to induce M1-like microglia activation (Michelucci et al. 2009; Dhawan et al. 2012). Here, we investigated whether interference with actin dynamics influences the uptake of oligomeric Aβ (1–42) by primary postnatal microglia and alters the subsequent transcription of pro-inflammatory molecules such as *iNos*. Compared to non-treated cells (dashed line in Fig. 2g), incubation with cytoskeletal drugs
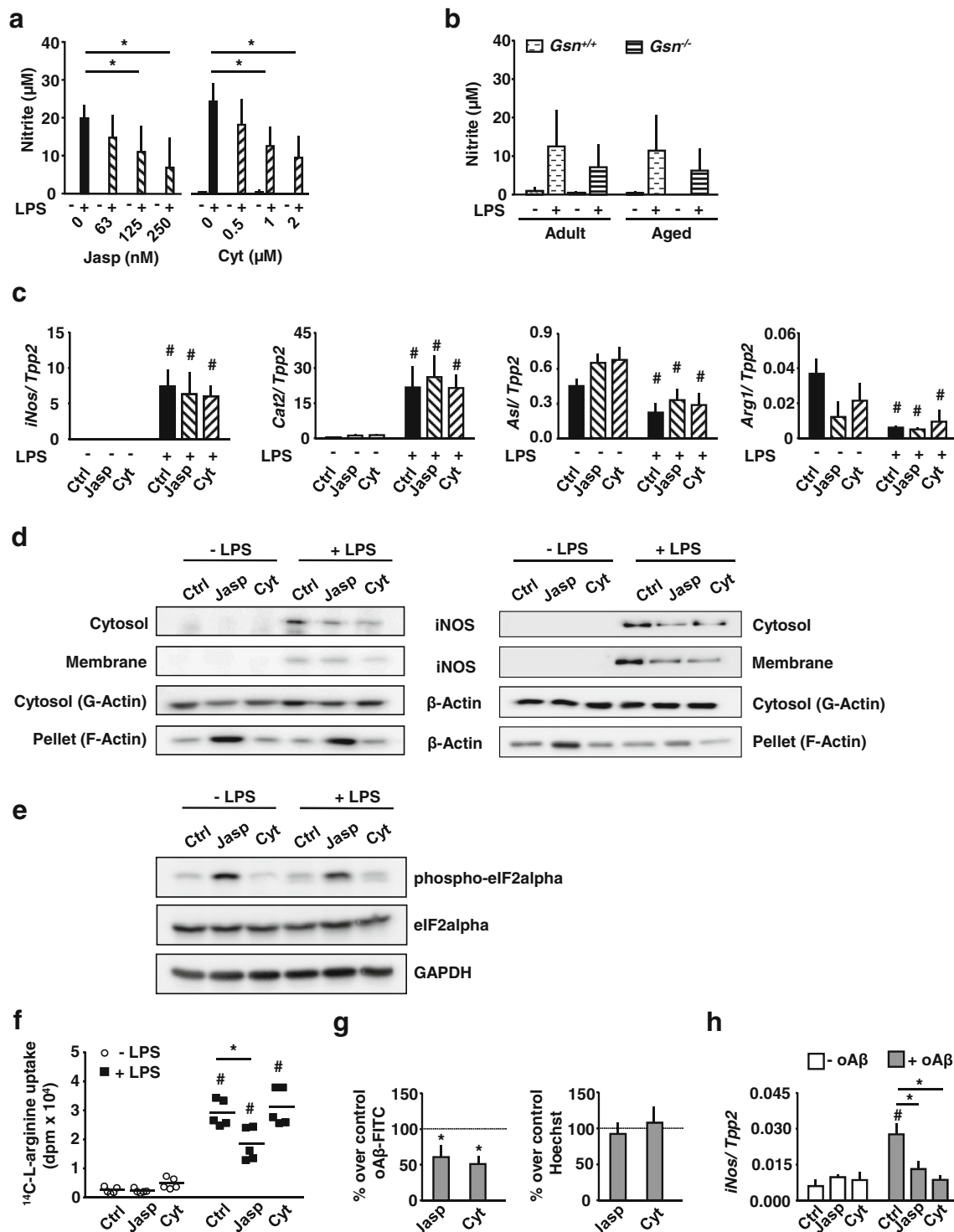
led to reduced phagocytosis of FITC-labelled oligomeric Aβ. Nuclear counterstaining was performed to confirm equal seeding densities (Fig. 2g). In keeping with reduced phagocytosis of Aβ (1–42), cells treated with cytoskeletal drugs also displayed reduced *iNos* mRNA transcription after 6-h incubation with Aβ (Fig. 2h).

Disruption of actin filament dynamics differentially affects 'conventional' and 'unconventional' cytokine release from LPS-activated microglia

TNFalpha and IL-6 represent cytokines following the so-called conventional secretory pathway characterized by
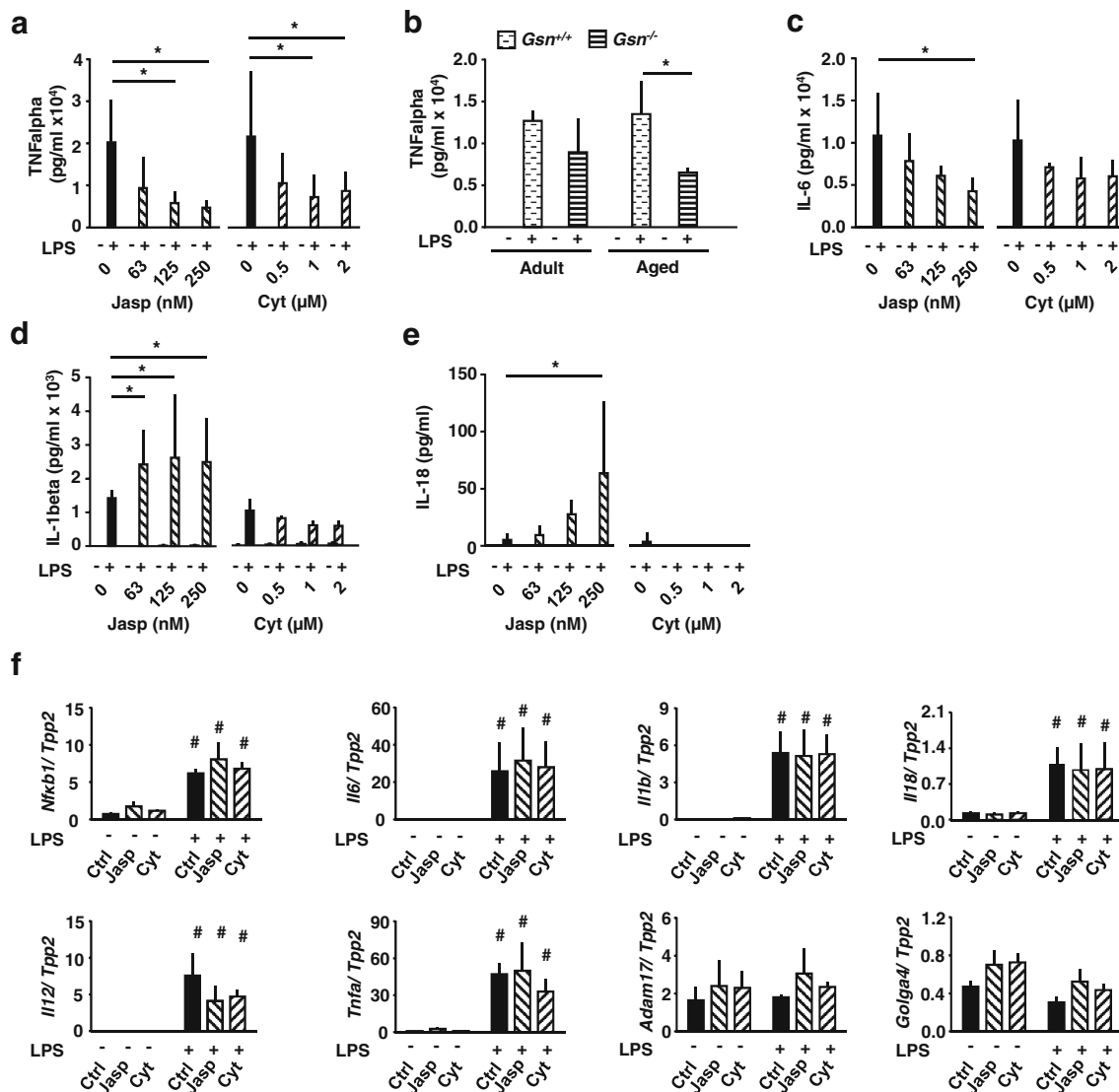
Fig. 3 Actin filament dynamics and cytokine release. Disruption of actin filament dynamics impairs conventional cytokine release. TNFalpha release from primary postnatal microglia (a) as well as from microglia cultured from adult (<6 months) and aged (>16 months) $Gsn^{+/+}$ and $Gsn^{-/-}$ brains (b) was measured after 6 h incubation with LPS (1 μg/ml). c IL-6 release and d IL-1beta release from primary postnatal microglia was measured after 6 and 24 h incubation with LPS (1 μg/ml), respectively. d Actin filament stabilization with jasplakinolide significantly increases IL-1beta release (unconventional pathway of cytokine release). e Strong IL-18 release from 24 h LPS activated microglia treated with actin polymerizing agent jasplakinolide. f mRNA expression of key genes associated with classical microglia activation after 6 h incubation with LPS (1 μg/ml) and/or cytoskeletal drugs (cytochalasin D, 2 μM; jasplakinolide, 250 nM). While LPS strongly induced mRNA transcription of genes associated with microglia activation, we did not observe any significant effect of either cytoskeletal drug. $N = 3–5$ independent measurements per data point. One-way ANOVA followed by Dunnett's post hoc test (a, c, d, e) or two-way ANOVA followed by Tukey's multiple comparisons test (b, f). *$p < 0.05$ within LPS/non-LPS treatment condition; #$p < 0.05$ between LPS and non-LPS treatment condition

synthesis in the endoplasmic reticulum and Golgi complex and subsequent membrane-bound transport to the cell surface (Lacy and Stow 2011). TNFalpha release from activated primary postnatal mouse microglia was significantly and dose-dependently inhibited by both jasplakinolide and cytochalasin D (Fig. 3a) after 6-h stimulation. A relatively similar pattern of effects was noted when IL-6 release was measured (Fig. 3c).

Furthermore, increased actin filament stabilization also impaired TNFalpha release from LPS-stimulated microglia harvested from adult and even more so from aged gelsolin-deficient brain (Fig. 3b). By contrast, IL-1beta and IL-18 are synthesized in the cytoplasm and released via non-classical routes (Hanamsagar et al. 2011; Lacy and Stow 2011). As expected, LPS activation increased IL-1beta and IL-18 levels in the cell culture supernatant. Interestingly,
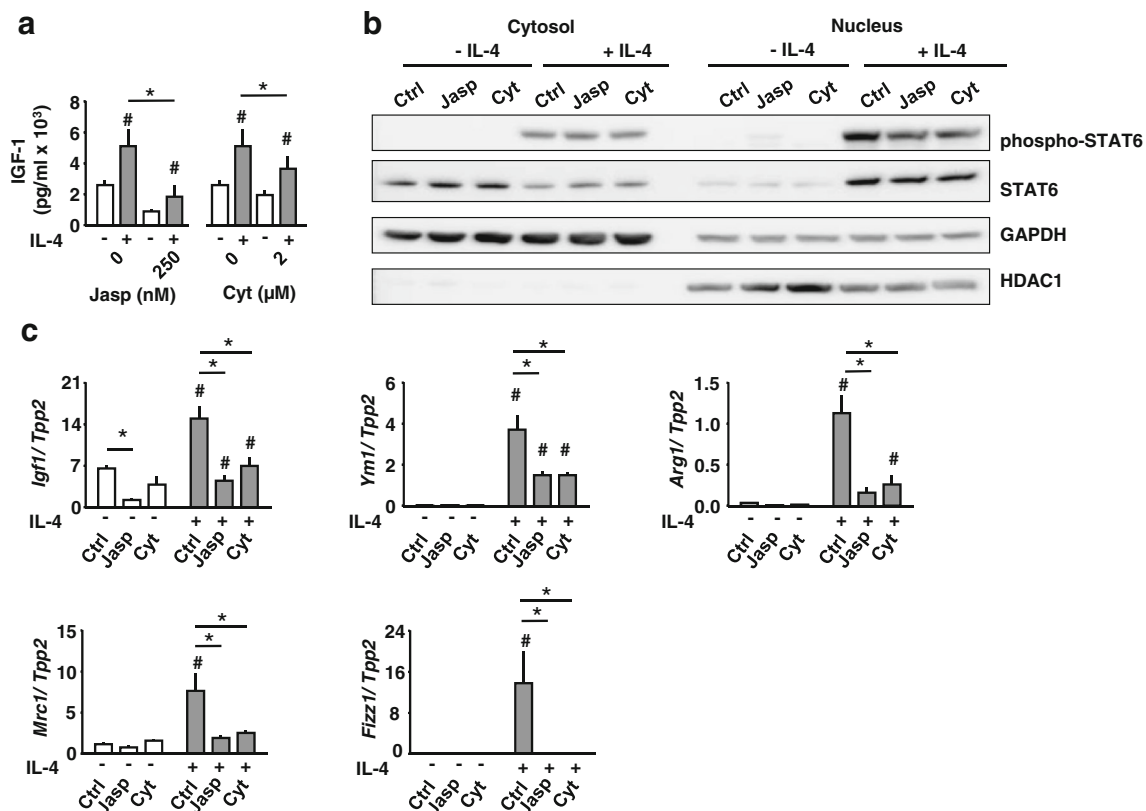
Fig. 4 Actin filament dynamics and alternative microglia activation. **a** IGF-1 release after 24 h incubation of primary microglia with IL-4. **b** BV-2 microglia were stimulated with IL-4 for 60 min. IL-4 stimulation resulted in increased levels of phospho-STAT6 in the nucleus. The IL-4 induced increase in pSTAT-6 levels in the nucleus was attenuated in the presence of cytoskeletal drugs. **c** Cytoskeletal drugs (jasplakinolide, 250 nM; cytochalasin D, 2 μM) inhibit transcription of IGF-1 and key genes implicated in alternative activation of microglia. $N = 4$–5 independent measurements per data point. Two-way ANOVA followed by Tukey's multiple comparisons test. *$p < 0.05$ within IL-4/non-IL-4 treatment condition; [#]$p < 0.05$ between IL-4 and non-IL-4 treatment condition

treatment with jasplakinolide led to further increases in the secretion of IL-1beta (Fig. 3d). Remarkably, strong release of IL-18 could only be detected after LPS stimulation in conjunction with actin filament stabilization (Fig. 3e).

Again, the effects of altered actin turnover on cytokine release were not regulated at the transcriptional level (Fig. 3f). Although all pro-inflammatory genes tested (*Nfkb1*, *Il6*, *Il1b*, *Il18*, *Il12*, *Tnfa*) were found to be strongly upregulated after LPS, disruption of actin dynamics did not produce any further effects. *Adam17* and *Golga4* are genes encoding proteins involved in the processing and trafficking of TNFalpha. *Adam17* and *Golga4* were not affected by either LPS activation or treatment with cytoskeletal drugs (Fig. 3f).

Disruption of actin filament dynamics impairs IL-4/STAT6 signalling and transcription of IL-4 responsive genes

IL-4 was used to induce the alternative microglia activation state. A strong increase in insulin-like growth factor 1 (IGF-1) release was seen in IL-4 induced primary postnatal microglia (Fig. 4a). Disruption of actin filament dynamics attenuated IGF-1 production (Fig. 4a). This was paralleled by decreased mRNA transcription of *Igf1* as well as of other M2-specific genes such as *Ym1*, *Arg1, Mrc1* and *Fizz1* (Fig. 4c). To further pinpoint the site of action of the actin agents, the IL-4/STAT6 signalling pathway upstream of the transcription of IL-4 responsive genes was investigated (Goenka and Kaplan 2011; Maier et al. 2012). After phosphorylation of STAT6 by Janus kinases (JAKs), phospho-STAT6 is translocated into the nucleus to act as a transcriptional activator (Nelms et al. 1999; Gordon and Martinez 2010; Zhou et al. 2012). IL-4/STAT6 signalling was analysed in BV2 microglia by monitoring (1) STAT6 phosphorylation in the cytosol and (2) the accumulation of transcription factor pSTAT6 in the nucleus after 60-min activation with IL-4. Neither cytoskeletal drug impacted STAT6 phosphorylation in the cytosol. The amount of phospho-STAT6 in the nuclear fraction was robustly increased after IL-4 stimulation. However, disruption of actin dynamics led to reduced phospho-STAT6 levels in the

nucleus (Fig. 4b). Taken together, the effects of altered actin turnover on the M2 phenotype relate to impaired IL-4-/STAT6 signalling resulting in reduced transcription of M2-specific genes (Fig. 4c).

Disruption of actin filament dynamics impairs microglia chemotaxis, phagocytosis and proliferation

Migration, phagocytosis and proliferation constitute core elements of microglial behaviour (Hanisch and Kettenmann 2007). To analyse the effect of impaired actin dynamics on microglial migration, we used the Boyden Chamber microchemotaxis model. Primary mouse microglia were treated with either jasplakinolide (250 nM) or cytochalasin D (2 μM) alone or in combination with the chemoattractant agent ADP (100 μM). Neither cytoskeletal drug exerted a significant effect on constitutive microglial migration as compared to the control condition. However, ADP-induced chemotaxis was reduced by >50 % in the presence of actin toxins (Fig. 5a). Chemotaxis of microglia derived from adult and aged $Gsn^{-/-}$ mice was also significantly reduced without an additional effect of the factor age (Fig. 5b). Similarly, phagocytosis of bacterial particles was impaired when actin turnover was disrupted pharmacologically or through gelsolin deficiency (Fig. 5c, d). Finally, we studied growth characteristics of cultured adult microglia derived from wild-type and $Gsn^{-/-}$ mice over a period of 4 weeks. Since microglia and astrocytes are cultivated in the same dish, this genetic approach allowed us to specifically address the effects of impaired actin dynamics in microglia (see also Supplementary Figure 1). Again, impaired actin turnover impeded microglia growth in culture (Fig. 5e).

Finally, we studied the implications of pathological actin filament stabilization for microglia behaviour in vivo. So far, neuropathological analyses of the brain of $Gsn^{-/-}$ mice have yielded no overt anatomic abnormalities (Endres et al. 1999; Yildirim et al. 2008; Kronenberg et al. 2010). Here, we investigated microglia densities in hippocampus and striatum of adult (<6 months) and aged (>16 months) $Gsn^{+/+}$ and $Gsn^{-/-}$ mice. Microglia densities did not differ between genotypes. However, a significant increase in Iba1-immunoreactive cells was detected as a consequence of ageing (Supplementary Figure 2).

Facial nerve axotomy results in the proliferation of resident microglia in the ipsilateral facial motor nucleus in the absence of infiltrating hematogenous cells (Kreutzberg 1996). Using microglia marker Iba1, we quantified microglia densites 3 days after facial nerve axotomy. Mice of either genotype showed an increase in the number of Iba1-immunoreactive cells in the ipsilateral facial nucleus. However, the increase in $Gsn^{-/-}$ mice was clearly reduced (Fig. 5f).

Fig. 5 Actin filament dynamics, microglia chemotaxis, phagocytosis and proliferation. Microglial migration was measured in a modified Boyden chamber chemotaxis assay in combination with ADP (100 μM) over a time period of 6 h. The migration rate was normalized to basal migration (DMEM only, 100 %). Pharmacological disruption of actin dynamics in primary postnatal microglia (**a**) as well as gelsolin deficiency in microglia derived from adult and aged brain resulted in a significant reduction in migratory capacity (**b**). Phagocytosis was measured based on the uptake of bacterial particles conjugated to pH-sensitive dye over 2 h. Pharmacological disruption of actin dynamics in primary postnatal microglia (**c**) as well as gelsolin deficiency in microglia harvested from adult and aged brain (**d**) resulted in a significant impairment of phagocytosis. **e** Growth characteristics of cultured primary microglia harvested from adult and aged brain. Microglia numbers were assessed by cell counting in a Fuchs–Rosenthal chamber after shake-off from the astrocytic feeder layer. $N = 3$ independent measurements per data point. One-way ANOVA followed by Dunnett's multiple comparison test (**a**, **c**) or two-way ANOVA followed by Tukey's multiple comparison test (**b**, **d**, **e**), $*p < 0.05$. **f** Microglia densities in the contralateral and ipsilateral facial nuclei of $Gsn^{+/+}$ and $Gsn^{-/-}$ mice were quantified using Iba1 staining. Representative images of Iba1 immunoreactivity 3 days after facial nerve axotomy. Results are expressed as the increase (in %) in the ipsilateral nucleus over the contralateral side. $N = 5$ animals per group. $*p < 0.05$, unpaired student's t test. *Scale bar* 50 μm. **g** Reduced proliferation of Iba1$^+$ cells (*green*) in the peri-ischaemic area of $Gsn^{-/-}$ mice at 3 days after 30 min MCAo/reperfusion. *Red* DNA synthesis marker BrdU. $*p < 0.05$, unpaired student's t test. $N = 4$–5 animals per group. *Scale bar* 40 μm

The peri-ischaemic area is quickly populated by Iba1-positive monocytic cells at early time points after ischaemic reperfusion injury to the brain (Farber et al. 2008). We, therefore, also investigated the effects of pathological actin filament stabilization on the percentage of Iba1+ cells that showed BrdU labelling in a well-established model of mild brain ischaemia [30 min middle cerebral artery occlusion (MCAo)/reperfusion]. Mice received five BrdU injections at 12-h intervals starting after induction of MCAo. Animals were killed after 72 h. The percentage of Iba1$^+$ cells showing BrdU labelling was significantly reduced in $Gsn^{-/-}$ as compared to $Gsn^{+/+}$ mice (Fig. 5g; analysis of 100 randomly selected Iba1$^+$ cells located in the border zone of the infarct per animal).

Increased intracellular Ca^{2+} levels in microglia harvested from $Gsn^{-/-}$ brain

Calcium is a common and versatile second messenger in microglia (Farber and Kettenmann 2006). Here, we monitored intracellular Ca^{2+} ([Ca^{2+}]$_{int}$) levels in microglia harvested from adult and aged brain of $Gsn^{+/+}$ and $Gsn^{-/-}$ mice (Fig. 6). Baseline and ATP-induced [Ca^{2+}]$_{int}$ was significantly higher in gelsolin-deficient microglia (Fig. 6b). Furthermore, the ATP-induced increase in [Ca^{2+}]$_{int}$ was higher in the aged microglia derived from $Gsn^{-/-}$ relative to wild-type brain (Fig. 6c).
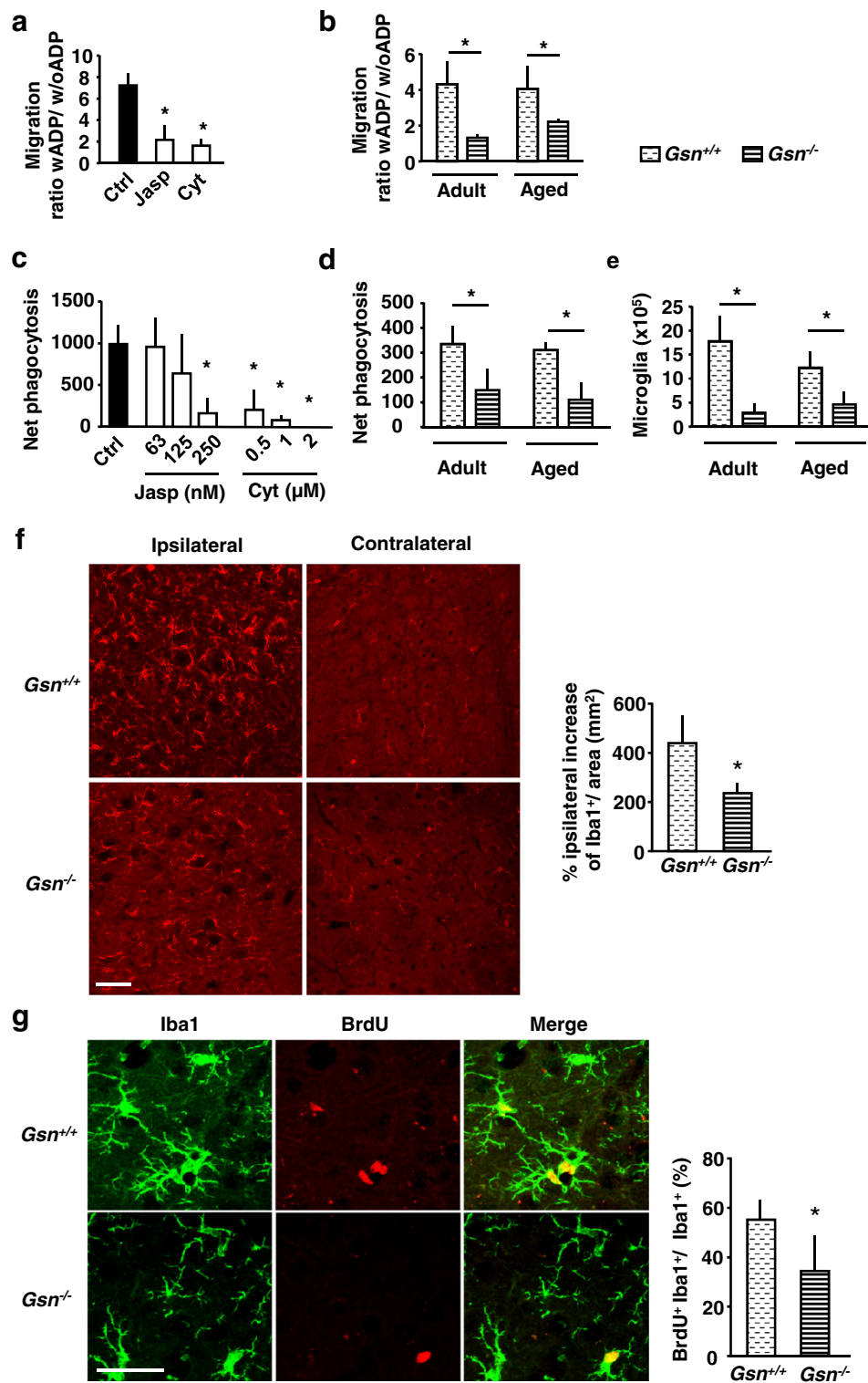
Discussion

In the present study, we manipulated the actin cytoskeleton and determined, as read-outs, the respective effects on the different activation patterns of microglia. Our study yielded the following major findings: (1) Disruption of actin dynamics in LPS-activated microglia inhibits NO release and reduces the secretion of TNFalpha and IL-6, two prototype molecules falling into the category of conventional cytokine release (Lacy and Stow 2011). By contrast,
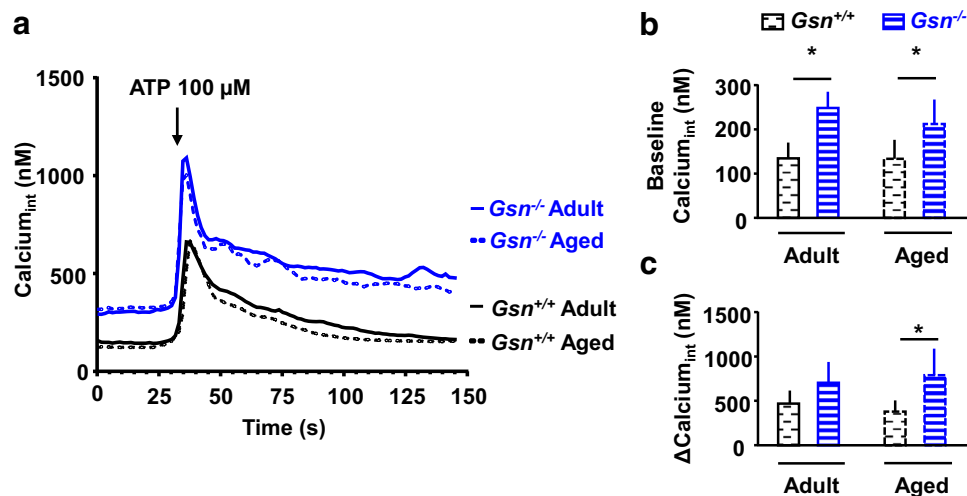
Fig. 6 Decreased baseline and ATP-evoked intracellular Ca^{2+} concentration in gelsolin-deficient microglia. Ex vivo isolated microglia derived from adult (<6 months) and aged (>16 months) $Gsn^{+/+}$ and $Gsn^{-/-}$ mice were studied 24 h after seeding. **a** Representative [Ca^{2+}]$_{int}$ traces from the four experimental groups. **b** Baseline [Ca^{2+}]$_{int}$ is higher in $Gsn^{-/-}$ as compared to $Gsn^{+/+}$ microglia. **c** Furthermore, the increase in [Ca^{2+}]$_{int}$ following 100 μm ATP is significantly higher in aged $Gsn^{-/-}$ as compared to $Gsn^{+/+}$ microglia. Two-way ANOVA followed by Tukey's multiple comparison tests. $N = 14$–26 from at least three independent experiments per condition. At the end of experiments, cells were exposed to calcium ionophore ionomycin to corroborate the responsiveness of the cells as well as of the detection system

increased actin filament stabilization promotes the secretion of IL-1beta and IL-18, which are produced in the cytoplasm and released by way of nonclassical routes (Lacy and Stow 2011). Importantly, all of these effects of actin dysregulation on the behaviour of M1 microglia were not related to altered transcription of M1 genes such as *Nfkb1*, *iNos*, *Tnfa*, *Il1b*, *Il6*, *Il12* and *Il18*. (2) Disruption of actin filament dynamics impairs IL-4/STAT6 signalling. This leads to decreased mRNA transcription of key M2-specific genes such as *Igf1*, *Ym1*, *Fizz1*, *Mrc1* and *Arg1*. Correspondingly, release of IGF-1, a crucial trophic factor derived from M2 microglia (Ueno et al. 2013), was markedly reduced when actin dynamics were disrupted. (3) In general agreement with earlier studies in macrophages, impaired actin dynamics lead to reduced microglia chemotaxis, proliferation and phagocytosis (e.g. de Oliveira and Mantovani 1988; Allen et al. 1997, 1998; Jonsson et al. 2012; Iqbal et al. 2013).

The actin cytoskeleton is sensitive to oxidative stress, which may lead to oxidation of exposed cysteine residues, disulphide bonds and, ultimately, reduced dynamic cytoskeletal plasticity (Bencsath et al. 1996; Dalle-Donne et al. 2001; Haarer and Amberg 2004). Furthermore, both Aβ and tau have been demonstrated to promote actin polymerization (Fulga et al. 2007; Henriques et al. 2010; Frandemiche et al. 2014). The results gathered here, therefore, have a direct bearing on our understanding of the role of impaired actin dynamics in age-dependent neurodegeneration and Alzheimer's pathogenesis. Interestingly, functional impairments in microglia motility and

phagocytic activity reminiscent of the effects of actin dysregulation reported here have recently been observed in mice with Alzheimer-like neuropathology. Importantly, these impairments coincided with β-amyloid deposition and were reversible with an amyloid-lowering intervention by Aβ vaccination (Krabbe et al. 2013).

It is generally held that a perturbation in the homeostasis of Aβ is intricately involved in the pathogenesis of Alzheimer's disease. In line with an earlier report (Mandrekar et al. 2009), we also found that disruption of actin filament dynamics markedly inhibited microglial uptake of oligomeric Aβ. Taken together, actin pathology in microglia may be partly cause and partly consequence of an Aβ dysequilibrium in the brain. Heterogeneous functional phenotypes of microglia ranging from classical to M2 activation in the brain of Alzheimer's disease patients as well as in Alzheimer's mouse models have been reported (Colton et al. 2006). Our results clearly suggest that impaired actin dynamics in cells shifting toward an M2 phenotype may dampen their neuroprotective capacity, e.g. by decreasing IGF-1 release. The diverse effects of altered actin dynamics on M1 microglia are more difficult to extrapolate to a disease context. However, it deserves mention that IL-1beta, which is induced by pathological actin filament stabilization, stimulates Aβ generation by γ-secretase-mediated cleavage of APP (Liao et al. 2004).

Inducible nitric oxide synthase, the NO producing enzyme in microglia and macrophages, is an essential inflammatory mediator (Brown and Neher 2010). It is the only NO synthase capable of producing micromolar

amounts of nitric oxide (Moss and Bates 2001). In macrophages, iNOS has been shown to associate with cortical actin. Furthermore, in line with our results, this peripheral iNOS colocalized with the cortical cytoskeleton was removed by disruption of actin dynamics (Webb et al. 2001). The current study demonstrates that actin dysregulation strongly inhibits NO release from LPS-stimulated microglia. It is a recurrent pattern in the findings reported here that the effects of cytoskeletal dysregulation on M1 microglia are not mediated at the transcriptional level. While LPS strongly induced mRNA expression of *iNos* and of substrate transporter *Cat2* and repressed mRNA transcription of urea cycle enzymes *Asl* and *Arg1*, actin disruption did not modify expression of these genes in activated microglia. Interestingly, however, iNOS protein expression after LPS stimulation, which was studied in both primary postnatal microglia and the immortalized murine BV2 microglial cell line, was reduced in the presence of cytoskeletal drugs. The substrate for iNOS is L-arginine, a semi-essential amino acid that needs to be actively transported into the cell. In line with previous studies of macrophages and microglia, arginine transport via the cell membrane was found to be increased after LPS stimulation (Kawahara et al. 2001; Yeramian et al. 2006). This initial crucial step in the activation of the nitric oxide pathway was significantly inhibited by pathological actin filament stabilization. This finding may also partly explain reduced iNOS protein levels in the presence of cytoskeletal drugs. Translational control of iNOS protein expression by arginine concentrations via negative regulation of eIF2alpha phosphorylation status has previously been demonstrated (Lee et al. 2003). In line with this earlier report and the results of the L-(14C)-arginine uptake assay, we found increased levels of phosphorylated eIF2alpha in activated microglia in the presence of actin stabilizer jasplakinolide. However, considering the results we obtained with actin disruptor cytochalasin D, it has to be acknowledged that translational control of iNOS is likely not the only mechanism underlying the inhibitory effects of actin dysregulation on NO release from activated microglia.

How, if not at the transcriptional level, does the state of the actin cytoskeleton interfere with differential modes of cytokine release after classical microglia activation? IL-1beta and IL-18 maturation is under the control of caspase 1, which cleaves both pro-IL-1beta and pro-IL-18 (Yao et al. 1992; Prinz and Hanisch 1999; Walsh et al. 2014). IL-1beta and IL-18 are leaderless proteins whose release occurs via ectosomes and is regulated by intracellular Ca^{2+} levels (Semino et al. 2005; Carta et al. 2013; Prada et al. 2013). The mechanisms involved in unconventional cytokine secretion are thus quite akin to exocytotic neurotransmitter release from neurons. The increased release of both IL-1beta and IL-18 from activated microglia in the presence of jasplakinolide, therefore, fits well with our earlier finding of increased Ca^{2+} influx in gelsolin-deficient synaptosomes resulting in enhanced neurotransmitter release (Kronenberg et al. 2010). In contrast, synthesis and release of TNFalpha as well as of IL-6 involve the endoplasmic reticulum and the Golgi apparatus. Conventional cytokine release was dose-dependently inhibited by both cytoskeletal compounds. Diverse mechanisms may be at play here. For example, actin dysfunction has been demonstrated to affect both translation and degradation of *Il6* mRNA in airway epithelial cells (van den Berg et al. 2006). Furthermore, another study in a macrophage-like cell line found that actin dynamics influence post-Golgi trafficking of TNFalpha (Shurety et al. 2000).

In summary, our study demonstrates that actin dysfunction profoundly and distinctly affects microglia behaviours. Disruption of actin filament dynamics impedes IL-4/STAT6 signalling and thereby dampens M2 polarization of IL-4 stimulated microglia. This effect of altered actin turnover relates primarily to reduced transcription of alternative activation genes. By contrast, the role of actin dynamics in classical activation does not relate to modulation of gene transcription and shows a major divergence in the pattern of cytokine release between actin depolymerization and increased actin stabilization.

References

Aguzzi A, Barres BA, Bennett ML (2013) Microglia: scapegoat, saboteur, or something else? Science 339:156–161. doi:10.1126/science.1227901

Allen WE, Jones GE, Pollard JW, Ridley AJ (1997) Rho, Rac and Cdc42 regulate actin organization and cell adhesion in macrophages. J Cell Sci 110(Pt 6):707–720

Allen WE, Zicha D, Ridley AJ, Jones GE (1998) A role for Cdc42 in macrophage chemotaxis. J Cell Biol 141:1147–1157. doi:10.1083/jcb.141.5.1147

Azuma T, Witke W, Stossel TP, Hartwig JH, Kwiatkowski DJ (1998) Gelsolin is a downstream effector of rac for fibroblast motility. EMBO J 17:1362–1370. doi:10.1093/emboj/17.5.1362

Bencsath FA, Shartava A, Monteiro CA, Goodman SR (1996) Identification of the disulfide-linked peptide in irreversibly sickled cell beta-actin. Biochemistry 35:4403–4408. doi:10.1021/bi960063n

Brown GC, Neher JJ (2010) Inflammatory neurodegeneration and mechanisms of microglial killing of neurons. Mol Neurobiol 41:242–247. doi:10.1007/s12035-010-8105-9

Bubb MR, Spector I, Beyer BB, Fosen KM (2000) Effects of jasplakinolide on the kinetics of actin polymerization. An explanation for certain in vivo observations. J Biol Chem 275:5163–5170

Carta S, Lavieri R, Rubartelli A (2013) Different members of the IL-1 family come out in different ways: DAMPs vs. cytokines? Front Immunol 4:123. doi:10.3389/fimmu.2013.00123

Casella JF, Flanagan MD, Lin S (1981) Cytochalasin D inhibits actin polymerization and induces depolymerization of actin filaments formed during platelet shape change. Nature 293:302–305

Chromy BA, Nowak RJ, Lambert MP, Viola KL, Chang L, Velasco PT, Jones BW, Fernandez SJ, Lacor PN, Horowitz P, Finch CE, Krafft GA, Klein WL (2003) Self-assembly of Abeta(1-42) into globular neurotoxins. Biochemistry 42:12749–12760. doi:10.1021/bi030029q

Colton CA (2009) Heterogeneity of microglial activation in the innate immune response in the brain. J Neuroimmune Pharmacol 4:399–418. doi:10.1007/s11481-009-9164-4

Colton CA, Mott RT, Sharpe H, Xu Q, Van Nostrand WE, Vitek MP (2006) Expression profiles for macrophage alternative activation genes in AD and in mouse models of AD. J Neuroinflamm 3:27. doi:10.1186/1742-2094-3-27

Dalle-Donne I, Rossi R, Milzani A, Di Simplicio P, Colombo R (2001) The actin cytoskeleton response to oxidants: from small heat shock protein phosphorylation to changes in the redox state of actin itself. Free Radic Biol Med 31:1624–1632. doi:10.1016/S0891-5849(01)00749-3

de Oliveira CA, Mantovani B (1988) Latrunculin A is a potent inhibitor of phagocytosis by macrophages. Life Sci 43:1825–1830

Dhawan G, Floden AM, Combs CK (2012) Amyloid-beta oligomers stimulate microglia through a tyrosine kinase dependent mechanism. Neurobiol Aging 33:2247–2261. doi:10.1016/j.neurobiolaging.2011.10.027

Endres M, Fink K, Zhu J, Stagliano NE, Bondada V, Geddes JW, Azuma T, Mattson MP, Kwiatkowski DJ, Moskowitz MA (1999) Neuroprotective effects of gelsolin during murine stroke. J Clin Invest 103:347–354. doi:10.1172/JCI4953

Fa M, Orozco IJ, Francis YI, Saeed F, Gong Y, Arancio O (2010) Preparation of oligomeric beta-amyloid 1-42 and induction of synaptic plasticity impairment on hippocampal slices. J Vis Exp. doi:10.3791/1884

Farber K, Kettenmann H (2006) Functional role of calcium signals for microglial function. Glia 54:656–665. doi:10.1002/glia.20412

Farber K, Markworth S, Pannasch U, Nolte C, Prinz V, Kronenberg G, Gertz K, Endres M, Bechmann I, Enjoji K, Robson SC, Kettenmann H (2008) The ectonucleotidase cd39/ENTPDase1 modulates purinergic-mediated microglial migration. Glia 56:331–341. doi:10.1002/glia.20606

Frandemiche ML, De Seranno S, Rush T, Borel E, Elie A, Arnal I, Lante F, Buisson A (2014) Activity-dependent tau protein translocation to excitatory synapse is disrupted by exposure to amyloid-beta oligomers. J Neurosci 34:6084–6097. doi:10.1523/JNEUROSCI.4261-13.2014

Freyer D, Manz R, Ziegenhorn A, Weih M, Angstwurm K, Docke WD, Meisel A, Schumann RR, Schonfelder G, Dirnagl U, Weber JR (1999) Cerebral endothelial cells release TNF-alpha after stimulation with cell walls of Streptococcus pneumoniae and regulate inducible nitric oxide synthase and ICAM-1 expression via autocrine loops. J Immunol 163:4308–4314

Fulga TA, Elson-Schwab I, Khurana V, Steinhilb ML, Spires TL, Hyman BT, Feany MB (2007) Abnormal bundling and accumulation of F-actin mediates tau-induced neuronal degeneration in vivo. Nat Cell Biol 9:139–148. doi:10.1038/ncb1528

Furukawa K, Fu W, Li Y, Witke W, Kwiatkowski DJ, Mattson MP (1997) The actin-severing protein gelsolin modulates calcium channel and NMDA receptor activities and vulnerability to excitotoxicity in hippocampal neurons. J Neurosci 17:8178–8186

Glass R, Synowitz M, Kronenberg G, Walzlein JH, Markovic DS, Wang LP, Gast D, Kiwit J, Kempermann G, Kettenmann H (2005) Glioblastoma-induced attraction of endogenous neural precursor cells is associated with improved survival. J Neurosci 25:2637–2646. doi:10.1523/JNEUROSCI.5118-04.2005

Goddette DW, Frieden C (1986) The kinetics of cytochalasin D binding to monomeric actin. J Biol Chem 261:15970–15973

Goenka S, Kaplan MH (2011) Transcriptional regulation by STAT6. Immunol Res 50:87–96. doi:10.1007/s12026-011-8205-2

Gordon S, Martinez FO (2010) Alternative activation of macrophages: mechanism and functions. Immunity 32:593–604. doi:10.1016/j.immuni.2010.05.007

Gourlay CW, Ayscough KR (2005) The actin cytoskeleton: a key regulator of apoptosis and ageing? Nat Rev Mol Cell Biol 6:583–589. doi:10.1038/nrm1682

Gourlay CW, Ayscough KR (2006) Actin-induced hyperactivation of the Ras signaling pathway leads to apoptosis in Saccharomyces cerevisiae. Mol Cell Biol 26:6487–6501. doi:10.1128/MCB.00117-06

Haarer BK, Amberg DC (2004) Old yellow enzyme protects the actin cytoskeleton from oxidative stress. Mol Biol Cell 15:4522–4531. doi:10.1091/mbc.E04-06-0445

Hanamsagar R, Torres V, Kielian T (2011) Inflammasome activation and IL-1beta/IL-18 processing are influenced by distinct pathways in microglia. J Neurochem 119:736–748. doi:10.1111/j.1471-4159.2011.07481.x

Hanisch UK, Kettenmann H (2007) Microglia: active sensor and versatile effector cells in the normal and pathologic brain. Nat Neurosci 10:1387–1394. doi:10.1038/nn1997

Hellmann-Regen J, Kronenberg G, Uhlemann R, Freyer D, Endres M, Gertz K (2013) Accelerated degradation of retinoic acid by activated microglia. J Neuroimmunol 256:1–6. doi:10.1016/j.jneuroim.2012.11.005

Henriques AG, Vieira SI, da Cruz ESEF, da Cruz ESOA (2010) Abeta promotes Alzheimer's disease-like cytoskeleton abnormalities with consequences to APP processing in neurons. J Neurochem 113:761–771. doi:10.1111/j.1471-4159.2010.06643.x

Holzinger A (2001) Jasplakinolide. An actin-specific reagent that promotes actin polymerization. Methods Mol Biol 161:109–120. doi:10.1007/978-1-60761-376-3_4

Iqbal AJ, Regan-Komito D, Christou I, White GE, McNeill E, Kenyon A, Taylor L, Kapellos TS, Fisher EA, Channon KM, Greaves DR (2013) A real time chemotaxis assay unveils unique migratory profiles amongst different primary murine macrophages. PLoS ONE 8:e58744. doi:10.1371/journal.pone.0058744

Jonsson F, Gurniak CB, Fleischer B, Kirfel G, Witke W (2012) Immunological responses and actin dynamics in macrophages are controlled by N-cofilin but are independent from ADF. PLoS ONE 7:e36034. doi:10.1371/journal.pone.0036034

Kawahara K, Gotoh T, Oyadomari S, Kajizono M, Kuniyasu A, Ohsawa K, Imai Y, Kohsaka S, Nakayama H, Mori M (2001) Co-induction of argininosuccinate synthetase, cationic amino acid transporter-2, and nitric oxide synthase in activated murine microglial cells. Brain Res Mol Brain Res 90:165–173. doi:10.1016/S0169-328X(01)00100-0

Koh JY, Choi DW (1987) Quantitative determination of glutamate mediated cortical neuronal injury in cell culture by lactate dehydrogenase efflux assay. J Neurosci Methods 20:83–90

Krabbe G, Halle A, Matyash V, Rinnenthal JL, Eom GD, Bernhardt U, Miller KR, Prokop S, Kettenmann H, Heppner FL (2013) Functional impairment of microglia coincides with Beta-amyloid

deposition in mice with Alzheimer-like pathology. PLoS ONE 8:e60921. doi:10.1371/journal.pone.0060921

Kreutzberg GW (1996) Microglia: a sensor for pathological events in the CNS. Trends Neurosci 19:312–318

Kronenberg G, Reuter K, Steiner B, Brandt MD, Jessberger S, Yamaguchi M, Kempermann G (2003) Subpopulations of proliferating cells of the adult hippocampus respond differently to physiologic neurogenic stimuli. J Comp Neurol 467:455–463. doi:10.1002/cne.10945

Kronenberg G, Wang LP, Synowitz M, Gertz K, Katchanov J, Glass R, Harms C, Kempermann G, Kettenmann H, Endres M (2005) Nestin-expressing cells divide and adopt a complex electrophysiologic phenotype after transient brain ischemia. J Cereb Blood Flow Metab 25:1613–1624. doi:10.1038/sj.jcbfm.9600156

Kronenberg G et al (2010) Impact of actin filament stabilization on adult hippocampal and olfactory bulb neurogenesis. J Neurosci 30:3419–3431. doi:10.1523/JNEUROSCI.4231-09.2010

Kwan W, Trager U, Davalos D, Chou A, Bouchard J, Andre R, Miller A, Weiss A, Giorgini F, Cheah C, Moller T, Stella N, Akassoglou K, Tabrizi SJ, Muchowski PJ (2012) Mutant huntingtin impairs immune cell migration in Huntington disease. J Clin Invest 122:4737–4747. doi:10.1172/JCI64484

Lacy P, Stow JL (2011) Cytokine release from innate immune cells: association with diverse membrane trafficking pathways. Blood 118:9–18. doi:10.1182/blood-2010-08-265892

Leadsham JE, Kotiadis VN, Tarrant DJ, Gourlay CW (2010) Apoptosis and the yeast actin cytoskeleton. Cell Death Differ 17:754–762. doi:10.1038/cdd.2009.196

Lee J, Ryu H, Ferrante RJ, Morris SM Jr, Ratan RR (2003) Translational control of inducible nitric oxide synthase expression by arginine can explain the arginine paradox. Proc Natl Acad Sci USA 100:4843–4848. doi:10.1073/pnas.0735876100

Liao YF, Wang BJ, Cheng HT, Kuo LH, Wolfe MS (2004) Tumor necrosis factor-alpha, interleukin-1beta, and interferon-gamma stimulate gamma-secretase-mediated cleavage of amyloid precursor protein through a JNK-dependent MAPK pathway. J Biol Chem 279:49523–49532. doi:10.1074/jbc.M402034200

Loisel TP, Boujemaa R, Pantaloni D, Carlier MF (1999) Reconstitution of actin-based motility of Listeria and Shigella using pure proteins. Nature 401:613–616. doi:10.1038/44183

Macleod CL, Kakuda DK (1996) Regulation of CAT: cationic amino acid transporter gene expression. Amino Acids 11:171–191. doi:10.1007/BF00813859

Maier E, Duschl A, Horejs-Hoeck J (2012) STAT6-dependent and -independent mechanisms in Th2 polarization. Eur J Immunol 42:2827–2833. doi:10.1002/eji.201242433

Mandrekar S, Jiang Q, Lee CY, Koenigsknecht-Talboo J, Holtzman DM, Landreth GE (2009) Microglia mediate the clearance of soluble Abeta through fluid phase macropinocytosis. J Neurosci 29:4252–4262. doi:10.1523/JNEUROSCI.5572-08.2009

Michelucci A, Heurtaux T, Grandbarbe L, Morga E, Heuschling P (2009) Characterization of the microglial phenotype under specific pro-inflammatory and anti-inflammatory conditions: effects of oligomeric and fibrillar amyloid-beta. J Neuroimmunol 210:3–12. doi:10.1016/j.jneuroim.2009.02.003

Morgan TE, Lockerbie RO, Minamide LS, Browning MD, Bamburg JR (1993) Isolation and characterization of a regulated form of actin depolymerizing factor. J Cell Biol 122:623–633

Moss DW, Bates TE (2001) Activation of murine microglial cell lines by lipopolysaccharide and interferon-gamma causes NO-mediated decreases in mitochondrial and cellular function. Eur J Neurosci 13:529–538. doi:10.1046/j.1460-9568.2001.01418.x

Nelms K, Keegan AD, Zamorano J, Ryan JJ, Paul WE (1999) The IL-4 receptor: signaling mechanisms and biologic functions. Annu Rev Immunol 17:701–738. doi:10.1146/annurev.immunol.17.1.701

Ni J, Dong Z, Han W, Kondrikov D, Su Y (2013) The role of RhoA and cytoskeleton in myofibroblast transformation in hyperoxic lung fibrosis. Free Radic Biol Med 61C:26–39. doi:10.1016/j.freeradbiomed.2013.03.012

Nishida Y, Sugahara-Kobayashi M, Takahashi Y, Nagata T, Ishikawa K, Asai S (2006) Screening for control genes in mouse hippocampus after transient forebrain ischemia using high-density oilgonucleotide array. J Pharmacol Sci 101:52–57. doi:10.1254/jphs.FP0050881

Olah M, Biber K, Vinet J, Boddeke HW (2011) Microglia phenotype diversity. CNS Neurol Disord Drug Targets 10:108–118. doi:10.2174/187152711794488575

Pannasch U, Farber K, Nolte C, Blonski M, Yan Chiu S, Messing A, Kettenmann H (2006) The potassium channels Kv1.5 and Kv1.3 modulate distinct functions of microglia. Mol Cell Neurosci 33:401–411. doi:10.1016/j.mcn.2006.08.009

Prada I, Furlan R, Matteoli M, Verderio C (2013) Classical and unconventional pathways of vesicular release in microglia. Glia 61:1003–1017. doi:10.1002/glia.22497

Prinz M, Hanisch UK (1999) Murine microglial cells produce and respond to interleukin-18. J Neurochem 72:2215–2218. doi:10.1046/j.1471-4159.1999.0722215.x

Scheffel J, Regen T, Van Rossum D, Seifert S, Ribes S, Nau R, Parsa R, Harris RA, Boddeke HW, Chuang HN, Pukrop T, Wessels JT, Jurgens T, Merkler D, Bruck W, Schnaars M, Simons M, Kettenmann H, Hanisch UK (2012) Toll-like receptor activation reveals developmental reorganization and unmasks responder subsets of microglia. Glia 60:1930–1943. doi:10.1002/glia.22409

Semino C, Angelini G, Poggi A, Rubartelli A (2005) NK/iDC interaction results in IL-18 secretion by DCs at the synaptic cleft followed by NK cell activation and release of the DC maturation factor HMGB1. Blood 106:609–616. doi:10.1182/blood-2004-10-3906

Shurety W, Merino-Trigo A, Brown D, Hume DA, Stow JL (2000) Localization and post-Golgi trafficking of tumor necrosis factor-alpha in macrophages. J Interferon Cytokine Res 20:427–438. doi:10.1089/107999000312379

Sun HQ, Yamamoto M, Mejillano M, Yin HL (1999) Gelsolin, a multifunctional actin regulatory protein. J Biol Chem 274:33179–33182

Ueno M, Fujita Y, Tanaka T, Nakamura Y, Kikuta J, Ishii M, Yamashita T (2013) Layer V cortical neurons require microglial support for survival during postnatal development. Nat Neurosci 16:543–551. doi:10.1038/nn.3358

van den Berg A, Freitas J, Keles F, Snoek M, van Marle J, Jansen HM, Lutter R (2006) Cytoskeletal architecture differentially controls post-transcriptional processing of IL-6 and IL-8 mRNA in airway epithelial-like cells. Exp Cell Res 312:1496–1506. doi:10.1016/j.yexcr.2006.01.010

Walsh JG, Muruve DA, Power C (2014) Inflammasomes in the CNS. Nat Rev Neurosci 15:84–97. doi:10.1038/nrn3638

Wang E, Gundersen D (1984) Increased organization of cytoskeleton accompanying the aging of human fibroblasts in vitro. Exp Cell Res 154:191–202. doi:10.1016/0014-4827(84)90679-7

Webb JL, Harvey MW, Holden DW, Evans TJ (2001) Macrophage nitric oxide synthase associates with cortical actin but is not recruited to phagosomes. Infect Immun 69:6391–6400. doi:10.1128/Iai.69.10.6391-6400.2001

Witke W, Sharpe AH, Hartwig JH, Azuma T, Stossel TP, Kwiatkowski DJ (1995) Hemostatic, inflammatory, and fibroblast responses are blunted in mice lacking gelsolin. Cell 81:41–51

Yao J, Keri JE, Taffs RE, Colton CA (1992) Characterization of interleukin-1 production by microglia in culture. Brain Res 591:88–93. doi:10.1016/0006-8993(92)90981-E

Yeramian A, Martin L, Serrat N, Arpa L, Soler C, Bertran J, McLeod C, Palacin M, Modolell M, Lloberas J, Celada A (2006) Arginine transport via cationic amino acid transporter 2 plays a critical regulatory role in classical or alternative activation of macrophages. J Immunol 176:5918–5924. doi:10.4049/jimmunol.176. 10.5918

Yildirim F, Gertz K, Kronenberg G, Harms C, Fink KB, Meisel A, Endres M (2008) Inhibition of histone deacetylation protects wildtype but not gelsolin-deficient mice from ischemic brain injury. Exp Neurol 210:531–542. doi:10.1016/j.expneurol.2007. 11.031

Zhou X, Spittau B, Krieglstein K (2012) TGFbeta signalling plays an important role in IL4-induced alternative activation of microglia. J Neuroinflamm 9:210. doi:10.1186/1742-2094-9-210